Available online at www.sciencedirect.com
SCIENCE DIRECT
Sensors and Actuators B 113 (2006) 36–46
SENSORS AND ACTUATORS B CHEMICAL
www.elsevier.com/locate/snb

Oxygen functionalisation of MWNT and their use as gas sensitive thick-film layers

R. Ionescu [a], E.H. Espinosa [a], E. Sotter [a], E. Llobet [a,*], X. Vilanova [a], X. Correig [a], A. Felten [b], C. Bittencourt [b], G. Van Lier [c], J.-C. Charlier [c,d], J.J. Pireaux [b]

[a] *Departament d'Enginyeria Electrònica, Universitat Rovira i Virgili, Campus Sescelades, Av. Països Catalans 26, 43007 Tarragona, Spain*
[b] *Laboratoire Interdisciplinaire de Spectroscopie Electronique, Facultés Universitaires Notre Dame de la Paix, 61 rue de Bruxelles, B-5000 Namur, Belgium*
[c] *Unité de Physico-Chimie et de Physique des Matériaux (PCPM), Université catholique de Louvain (UCL), Place Croix du Sud, 1 (Boltzmann), B-1348 Louvain-la-Neuve, Belgium*
[d] *Research Center in Micro- and Nanoscopic Materials and Electronic Devices (CERMIN), Université catholique de Louvain (UCL), B-1348 Louvain-la-Neuve, Belgium*

Received 9 December 2004; received in revised form 3 February 2005; accepted 7 February 2005
Available online 26 February 2005

Abstract

Multi-wall carbon nanotubes (MWNT) were functionalised in an oxygen-based atmosphere by an inductively coupled RF-plasma at 13.56 MHz. X-ray photoelectron spectroscopy analysis showed that the chemical composition of the nanotube surface depends on the plasma conditions used. The MWNT were then deposited onto microhotplate gas sensor substrates by the drop coating method. A well-adhered thick-film of carbon nanotubes mesh (~17 μm) was obtained after annealing in air. The influence of the different plasma conditions on the responsiveness of gas sensors fabricated with the functionalised MWNT was studied. The gas sensing properties were investigated both experimentally and theoretically for NO_2, and NH_3 at room temperature.

Keywords: MWNT functionalisation; Plasma treatment; Gas sensors; Drop coating; Room temperature sensing; Ab initio theoretical calculations

1. Introduction

In nature, carbon is one of the chemical elements that can take different allotropic forms, in particular graphite, diamond and fullerene [1]. Carbon nanotubes (CNT) are fullerene-like structures that were discovered a decade ago by Iijima [2]. Their applications' potential in many fields of science was anticipated from the very beginning and the number of researchers that are studying and implementing them increases every day. They have been employed in components of nanoelectronic technology [3], as probes in scanning probe microscopy [4], in high-sensitivity microbalances [5], in hydrogen storage devices [6], in field emission type displays [7], as electrodes in organic light-emitting diodes [8], as tiny tweezers for nanoscale manipulation [9], and as gas detectors [10].

Since their discovery, various methods have been developed to produce carbon nanotubes, including arc discharge [11], laser vaporisation [12], pyrolysis [13] and chemical vapour deposition [14]. Two general categories of CNT can be fabricated [15]. Specifically, single-wall carbon nanotubes (SWNT), which can be thought of as cylinders rolled from a graphitic sheet, and multi-wall carbon nanotubes (MWNT), which can be thought of as coaxial structures of various

* Corresponding author. Tel.: +34 977 558502; fax: +34 977 559605.
E-mail address: ellobet@etse.urv.es (E. Llobet).

0925-4005/$ – see front matter © 2005 Elsevier B.V. All rights reserved.
doi:10.1016/j.snb.2005.02.020

graphitic cylinders of different diameters. Depending of their chirality and diameter, the electronic structure of a CNT can be either metallic or semiconducting [15]. In practice it is difficult to obtain only semiconducting nanotubes from as grown samples, which are typically mixtures of both metallic and semiconducting CNT. Even when CNT are directly grown by a chemical vapour deposition (CVD) process, there is no control over the growth of semiconducting or metallic nanotubes [16].

Carbon nanotubes have been recently employed as active material in semiconductor gas sensors. The good potential of CNT for detecting gases arises from their very large surface area because of their central hollow cores and outside walls [17]. Recent studies have proved that CNT-based gas sensors can detect hazardous gases at low temperatures (e.g. below 200 °C), and even at room temperature [18–20]. This reduces the power consumption of the sensors and enables the safe detection of flammable gases in potentially explosive atmospheres. Therefore, this material is very promising as active layer for gas sensing applications.

However, the presence of a thick graphite-like layer (formed during the fabrication process) at the surface of nanotubes, which contributes with sp^2 electronic states, can rule out the sensing potential of this material. Moreover, the agglomeration of CNT into bundles during their synthesis appears as a technological difficulty for forming a well-dispersed active layer. The modification of the chemical composition at the surface of carbon nanotubes has been proved efficient at overcoming these drawbacks [21,22]. Furthermore, functionalising nanotubes allows their chemical compatibility with other materials. For example, they can be incorporated within polymers, attached to metals, or other materials, transferring their properties to the new composite material. Several methods, such as chemical [23], electrochemical [24], mechano-chemical [25] and plasma [26] treatments, can be applied to tailor the chemical composition of the nanotube surface. Among them, plasma treatments have the advantage of being non-polluting and providing a wide range of different functional groups depending on plasma parameters such as power, gases used, duration of treatment and pressure.

In this paper the responsiveness to nitrogen dioxide and ammonia of differently RF-plasma functionalised MWNT was investigated. The influence of the chemical composition of the nanotube surface on their sensing properties was also studied. X-ray photoelectron spectroscopy (XPS) was used to follow the changes in chemical composition induced at the surface of nanotubes due to the plasma treatment and scanning electron microscopy (SEM) was used to evaluate the dispersion of nanotubes.

These experimental results were compared to theoretical ab initio calculations in order to analyse the interaction between the carbon nanotube surface and the functional groups under consideration, as well as the role of defects on the functionalisation process.

2. Experimental

2.1. Plasma functionalisation

Four differently funtionalised MWNT were used to integrate the sensitive layer of microhotplate gas sensors. The active layers were prepared using commercially available (Nanocyl, S.A. [27]) multi-walled carbon nanotubes grown by CVD. The as-provided nanotubes were not purified (i.e. purity was higher than 65%), up to 50 μm in length and their outer and inner diameters ranged from 3 to 15 and 2 to 7 nm, respectively. In order to perform a uniform functionalisation, the nanotubes were placed inside a glass vessel and a magnet, externally controlled from the plasma chamber, was used to stir the nanotube powder during a plasma treatment. Inductively coupled plasma at a RF frequency of 13.56 MHz was used [28]. Once the CNT powder was placed inside the plasma glow discharge, the treatment was performed at a pressure of 0.1 Torr, using a power ranging from 30 to 100 W, and processing time was adjusted between 10 and 30 min. A controlled flow of oxygen was introduced inside the chamber. The excited species, radicals, electrons, ions and UV light within the plasma interacted with the surface of the CNT breaking the C–C bonds and creating active sites for bonding of functional groups. Thus, depending on the parameters used, it is possible to reduce the graphite-like layer at a point that the catalysts used in the fabrication of nanotubes are exposed at the surface.

Specifically, depending on the plasma treatment parameters used (shown in Table 1), four different types of oxygen functionalisation were performed. The nanotubes resulting from these treatments were employed as active layer for gas sensors.

2.2. Microhotplate substrates

Integrated microhotplates with arrays of four microsensors were fabricated (at the Centro Nacional de Microelectrónica, Barcelona, Spain) on double-side polished p-type ⟨1 0 0⟩ Si substrates, 300 μm thick (4–40 Ω cm). The structure of the device basically consists of the following stacked layers: a 300 nm thick Si_3N_4 layer grown by low pressure chemical vapour deposition (LPCVD), a $POCl_3$-doped polysilicon heating meander of 6 Ω/sq. of resistance, a 0.8 μm thick SiO_2 layer to insulate the heater from the electrodes and 200 nm thick Pt electrodes. A backside silicon

Table 1
Plasma treatment parameters used for MWNTs functionalisation and oxygen concentration in at.% measured by XPS after functionalisation

Functionalisation	Power (W)	Pressure (Torr)	Time (min)	O (%)
A	–	–	–	0
B	30	0.1	10	10
C	30	0.1	30	20
D	100	0.1	10	20

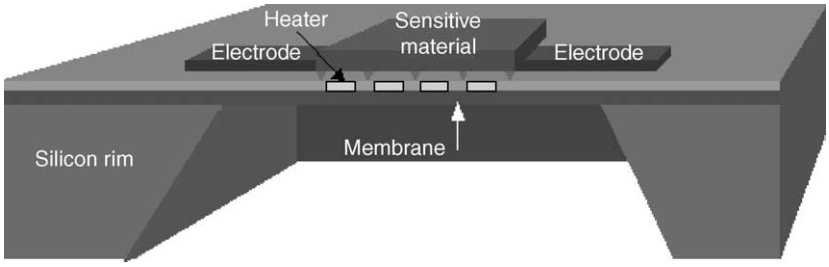

Fig. 1. Structure of the micromachined sensor.

etching with KOH at 70 °C (40 wt.%) was used to create four 900 μm × 900 μm thermally insulated membranes on each chip. Chips were mounted on TO-8 packages. A detailed description of the sensor substrates can be found elsewhere [29]. Fig. 1 shows the structure of the sensors.

2.3. MWNT deposition

The drop coating method was employed for depositing MWNT onto the sensor substrates [16]. A solution was prepared by dispersing MWNT in glycerol (25 mg in 1 ml). The dispersion and adequate mixture of the components were enhanced by stirring the solution in an ultrasonic bath. The resulting paste was then dropped onto the micromachined membranes using a microinjector (JBE1113 Dispenser, I&J FISNAR Inc., USA).

The deposited films were subsequently annealed in situ at 350 or 480 °C for 2 h. The purpose of this process was to ensure a good adherence of MWNT to the sensor substrates and to burn out the organic vehicle (i.e. glycerol) used for preparing the deposition paste. After the annealing process, the baseline resistance of the sensors, i.e. the resistance in dry air, ranged typically between 50 and 150 Ω.

Fig. 2 shows a picture of a four-element microhotplate array mounted on a standard TO-8. The MWNT thick films lying over the four electrode areas of the integrated array can be observed.

2.4. Material characterisation

X-ray photoelectron spectroscopy analyses were performed in order to evaluate the chemical change at the surface of MWNT. XPS measurements were performed with a HP 5950A system equipped with a hemispherical electron energy analyser. The photon source was a monochromatised Al Kα line ($h\nu$ = 1486.6 eV). The nominal resolution of the system (source + analyser) was 0.7 eV. In the spectrum analysis, the background signal was subtracted by Shirley's method. All binding energies were corrected for charging effect by calibration on the graphite C 1s peak at 284.6 eV. The C 1s spectrum analysis was carried out by fitting a graphite peak shape obtained in the same analysing conditions and other components with mixed (Gaussian + Lorentzian) line shapes.

The morphology of the MWNT based films deposited onto the microhotplate substrates was investigated by scanning electron microscopy. SEM measurements were performed using a Joel JSM 6400 equipment, with a resolution of 0.3 nm. The magnification during this study was set to values varying between 30,000 and 150,000. A voltage of 30 kV was applied for exciting the electrons that bombarded the surface under study. The system allows a sample rotation of 360° and a sample inclination of 90°.

2.5. Gas measurement system

Two four-element MWNT microarrays (each microarray had its four membranes coated with differently functionalised MWNT films, i.e. types A, B, C or D) were kept into a 10 ml test chamber. A continuous flow measurement system, based on computer-driven mass flow controllers, was used to generate the desired concentrations of NO_2 and NH_3 in dry air (79% N_2 and 21% O_2). The flow rate was set to 200 ml/min. The sensor resistances were acquired and stored in a PC using an Agilent 34970A data acquisition unit.

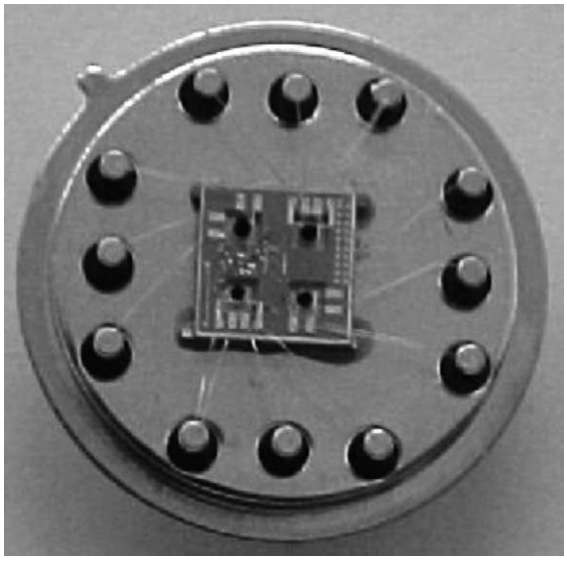

Fig. 2. Picture of a 4-element microhotplate sensor array based on drop-coated MWNT.

3. Computational details

In order to make a further interpretation of the experimental results, ab initio calculations were performed on a finite open single-walled (5,5) carbon nanotube with 150 carbon atoms and hydrogen termination at the open ends. As defects are supposed to play a key role in the chemical properties of carbon nanotubes, this system was also considered with a vacancy, i.e. one carbon atom removed from the middle of the structure (in order to minimise effects induced by open ends). Both systems (perfect and defective one) were functionalised with distinct oxygen and nitrogen containing functional groups (see below), and all systems under consideration were fully optimised at the ab initio restricted Hartree-Fock level of theory using a 3-21G basis set. The same level was used for all energy and property calculations, using the GAUSSIAN03 program [30].

Interaction energy E_{Int} was calculated as the difference in energy between the functionalised carbon nanotube (E_{Tot}) on the one hand, and the carbon nanotube without the functional group (E_{CN}) and the free standing functional group (E_{R}) on the other hand, using Eq. (1):

$$E_{\mathrm{Int}} = E_{\mathrm{Tot}} - (E_{\mathrm{CN}} + E_{\mathrm{R}}) \quad (1)$$

These energies were calculated from the fully optimised structures. The total charges for the calculations of the free standing functional group were taken the same as for the functionalised carbon nanotube (−1 or 0), the total

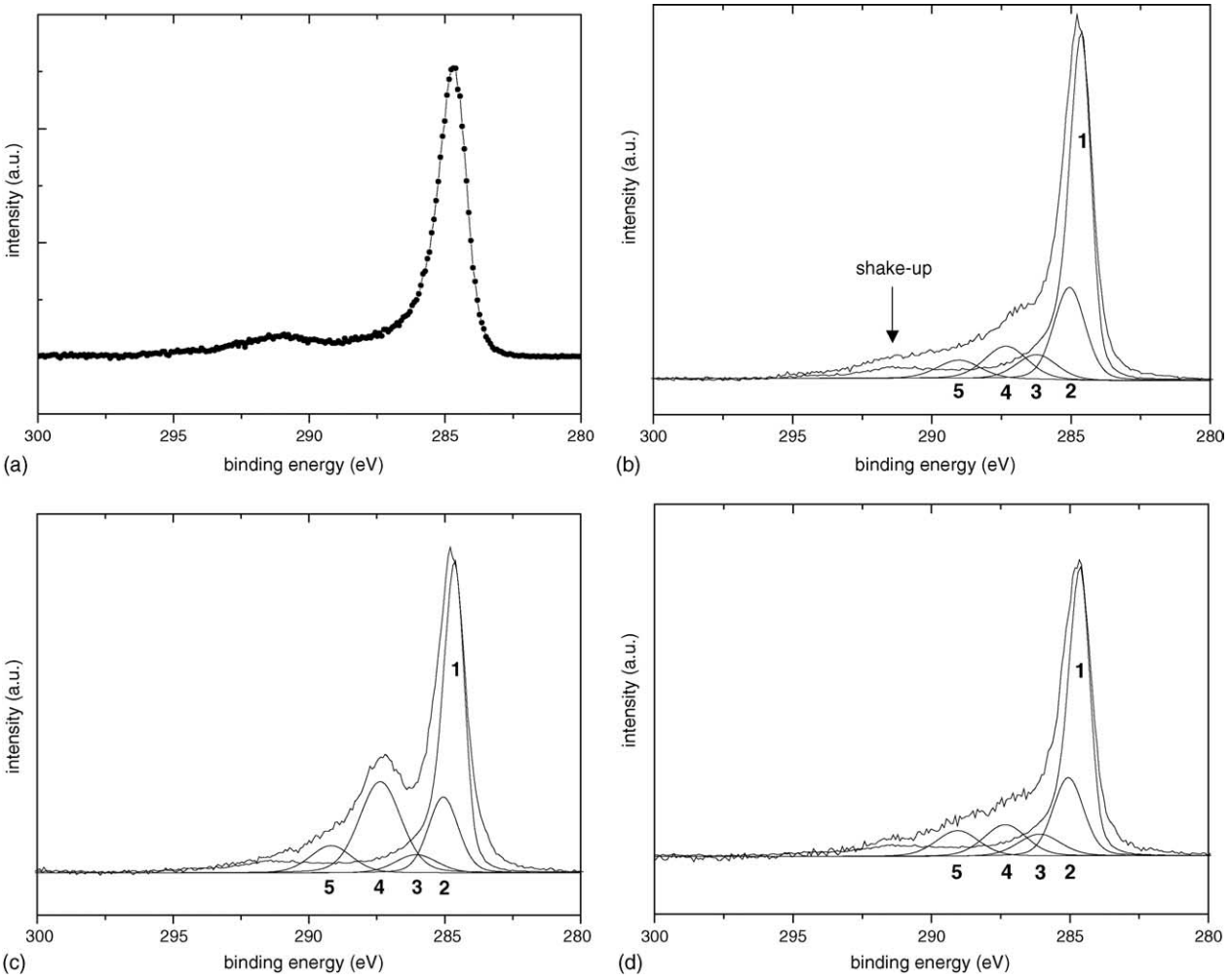

Fig. 3. (a) XPS C 1s core level spectrum recorded on as-grown nanotubes powder. (b) C 1s core level spectrum recorded on the nanotubes used for sensors type B. The main peak (1) at 284.6 eV corresponds to the graphite signal. Peak (2) centred at 285.1 eV is attributed to the sp^3 carbon atoms. Peaks (3) at 286.2 eV, (4) at 287.2 eV and (5) at 288.9 eV correspond to hydroxyl, carbonyl (or ether) and carboxyl (or ester) groups, respectively. (c) C 1s core level spectrum recorded on nanotubes used for sensors type C. The main peak (1) at 284.6 eV corresponds to the graphite signal. Peak (2) centred at 285.1 eV is attributed to the sp^3 carbon atoms. Peak (3) at 286.2 eV, (4) at 287.2 eV and (5) at 288.9 eV correspond to hydroxyl, carbonyl (or ether) and carboxyl (or ester) groups, respectively. (d) XPS C 1s core level spectrum recorded on sample D. The main peak (1) at 284.6 eV corresponds to the graphite signal. Peak (2) centred at 285.1 eV is attributed to the sp^3 carbon atoms. Peak (3) at 286.2 eV, (4) at 287.2 eV and (5) at 288.9 eV correspond to hydroxyl, carbonyl (or ether) and carboxyl (or ester) groups, respectively.

charge of the non-functionalised carbon nanotube was set to 0.

4. Results and discussion

4.1. Compositional and morphological analysis of the MWNT films

XPS analyses were performed in order to determine the chemical composition of the nanotube powders used to prepare the sensors. Fig. 3(a) shows the C 1s core level spectrum recorded on the as-provided nanotube powders (used for sensors type A). The full width half maximum (FWHM) of this peak is 1.1 eV; this value is higher than the expected for purified nanotube powders. However, this value is consistent with the one found for non-purified nanotube powders which is characterised not only by the presence of perfect nanotubes but also by defective ones and amorphous carbon [31]. A strong shake-up satellite (6 eV loss energy) with total intensity of about 5% is noticeable; the whole structure is taken into account in the quantitative analysis of the C 1s peak (see e.g. Fig. 3(b)–(d)).

Fig. 4(a) shows the XPS survey spectrum recorded on nanotube powders used for sensors type B (see Table 1 for the parameters of this specific functionalisation). This spectrum reveals the presence of carbon and oxygen on the sample. The concentration of oxygen evaluated by XPS was found to be 10%. Identifying the chemical modification produced by plasma treatment at the surface of nanotubes is straightforward when the C 1s core level spectrum is analysed (see Fig. 3(b)). This spectrum is made up of five components that can be decomposed into:

- A main peak (1) at 284.6 eV generated by photoelectrons emitted from carbon atoms in the graphite configuration, including its shake-up structure.
- A second peak centred at 285.1 eV (2), which can be attributed to photoelectrons emitted from carbon atoms with sp^3 configuration [31].
- Three other components centred at 286.2 eV (3), 287.2 eV (4) and 288.9 eV (5) generated by photoelectrons emitted from carbon atoms belonging to hydroxyl, carbonyl (or ether) and carboxyl (or ester) groups, respectively. The relative concentrations of these components are shown in Table 2.

Table 2
Relative concentration found for the five components forming the C 1s XPS spectrum

Sample	sp^2 (%)	sp^3 (%)	—C—O (%)	—C═O (%)	—COO (%)
A	76	14	–	–	–
B	58.5	18.5	7.3	9.6	6.1
C	57.4	12.5	2.6	22.4	5.1
D	63.7	16.4	5.2	8.3	6.4

Using the same parameters of the plasma for producing sample B (Table 1) but with increased exposure time results in sample C. Sample C shows a different distribution of the concentration of functional groups attached to the nanotube surface. As it can be derived by comparing Fig. 3(b) and (c), the same five components are present in both spectra. However, the amount of carbonyl groups (component at 287.2 eV) attached to the nanotube surface increases considerably. The relative concentrations of these five components are shown, once again, in Table 2.

When a stronger plasma treatment was used (sample type D, Table 1), a chemical etching of the nanotube surface occurred. The XPS survey spectrum (Fig. 4(b)) reveals the presence of photoelectrons emitted from transition metals (Co and Fe) and aluminium atoms, indicating that carbon atoms were removed from the nanotube surface by plasma. This results in the exposure of the previously encapsulated catalysts used to grow nanotubes. Fig. 3(d) shows the C 1s core level spectrum recorded on sample D; as for the previously analysed

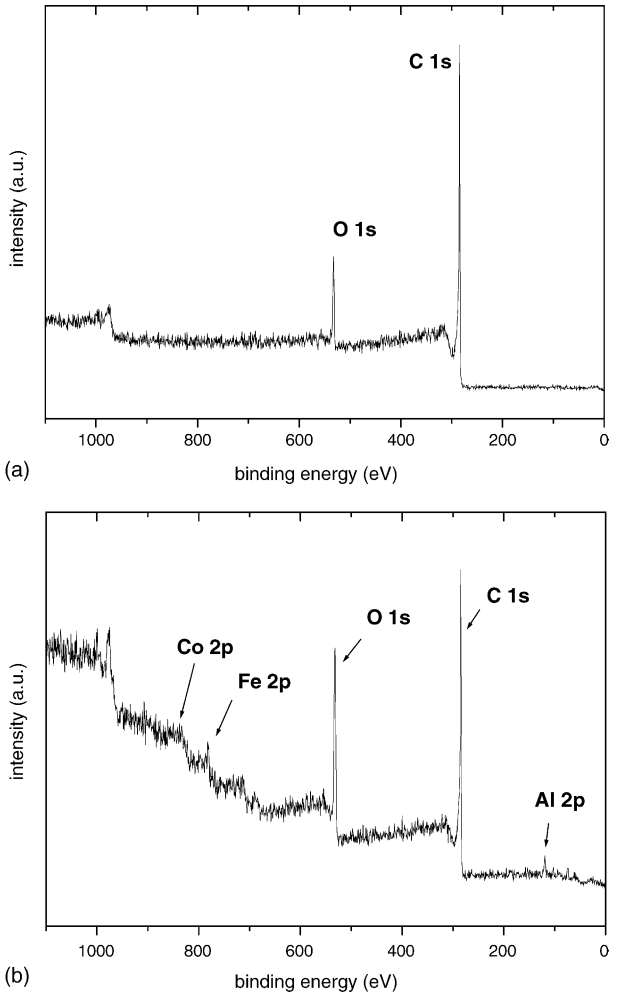

Fig. 4. (a) XPS survey spectrum recorded on the nanotubes used for sensors type B. (b) Survey spectrum recorded on nanotubes used for sensors type D. Photoelectrons generated from transition metals (Co and Fe) and aluminium atoms can be observed.

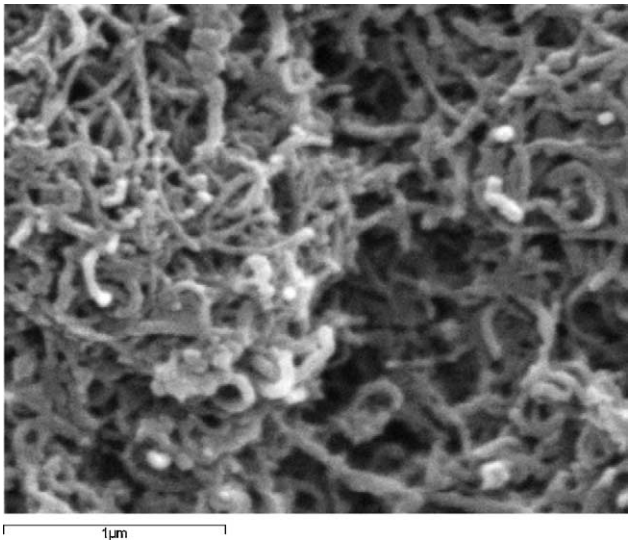

Fig. 5. SEM image of a MWNT film deposited over the sensor substrate.

samples, it is made up of the same five components, however, with a different distribution of concentrations (Table 2).

In summary, the XPS analysis revealed that after functionalisation, four different types of materials were obtained:

- Type A: non functionalised MWNT.
- Type B: MWNT with 10% oxygen at the surface.
- Type C: MWNT with 20% oxygen at the surface.
- Type D: MWNT with 20% oxygen + Co + Fe + Al.

A SEM analysis was performed in order to study the morphology of the MWNT films coating the sensor substrates after they had been annealed in situ (see Fig. 5). The SEM analysis did not reveal significant morphological changes between the differently functionalised nanotubes. The formation of a dispersed mesh of MWNT could be observed for the four differently functionalised materials analysed. SEM analyses indicated that well-adhered thick films were obtained, which had an average thickness near 17 μm. These results prove the correct deposition of the sensing material onto micromachined substrates.

4.2. Room temperature detection of NO_2 and NH_3

Next, the potential of MWNT-based chemical gas sensors for detecting hazardous gases at ambient temperature was investigated. Therefore, the performances of the sensors were tested for different concentrations of NO_2 and NH_3. Although the microhotplate substrates include an embedded resistor to heat the active area, sensors were operated at room temperature, i.e. 25 °C.

The best responses to NO_2 were obtained by sensors coated with films of types B and C. Fig. 6 shows the resistance changes experienced by sensors type B and C when operated at room temperature, after their exposure to successively increasing concentrations of NO_2 (500 ppb, 1, 5, and 10 ppm). These sensors were able to detect NO_2 at concentrations as

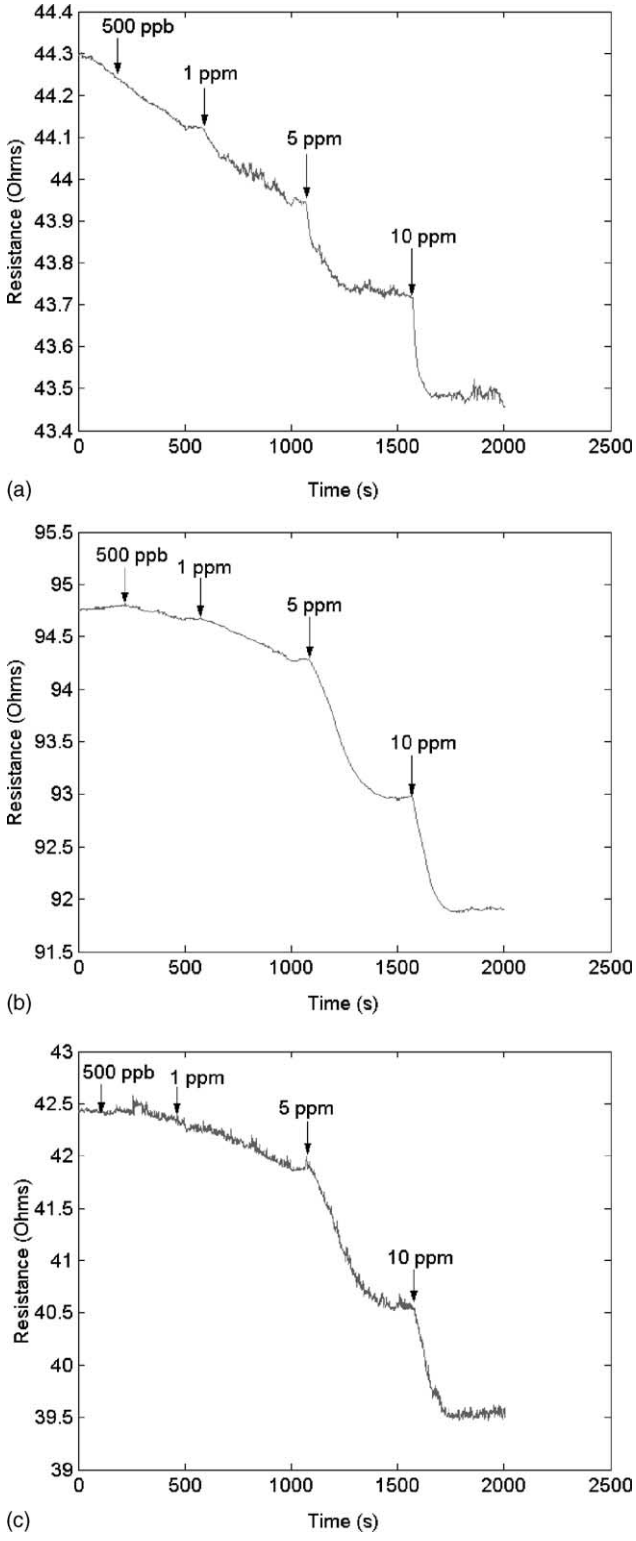

Fig. 6. Responses at room temperature to increasing concentrations of NO_2 of a sensor type B annealed at 350 °C (a), of a sensor type C annealed at 350 °C (b) and of a sensor type C annealed at 480 °C (c).

low as 500 ppb. In addition, sensors coated with films type A or D did not show responsiveness to NO_2 at concentrations below 10 ppm. This difference in responsiveness can be associated with the type of functional groups present at the surface of the nanotubes. It can be derived from Fig. 6 that the best responsiveness is found for sensors coated with films of type C, which is the functionalised sample that showed the highest concentration of C=O functional groups. Therefore, this functional group plays an important role in the sensitivity to nitrogen oxide species. The films behaved similarly to a p-type semiconductor in the presence of NO_2 (i.e. oxidising species), as their resistance decreased when detecting this gas.

The best sensitivity to NH_3 at room temperature was reached by sensors with an active layer of type D (see Fig. 7). This is probably due to the presence of catalytically active metals in samples D (i.e. Co, Fe and Al), which play an active role in the detection of ammonia. While sensors type D responded to NH_3 concentrations as low as 200 ppm, sensors type A, B or C could not detect NH_3 below 500 ppm and their responses were weak and slow. The films, once again, behaved as p-type semiconductors in the presence of NH_3 (i.e. reducing species), as their resistance increased when detecting this gas.

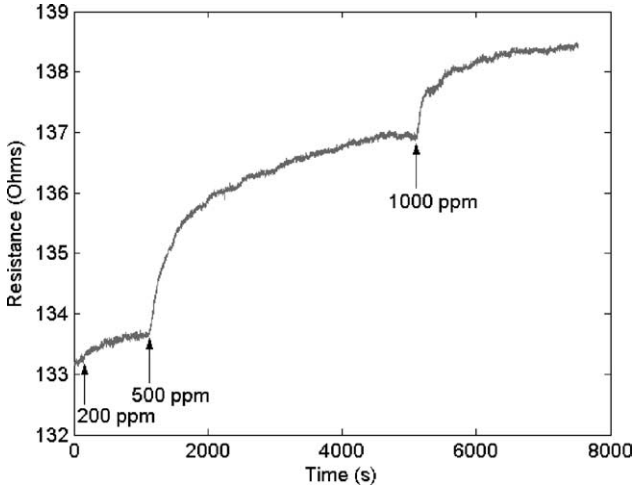

Fig. 7. Response at room temperature to increasing concentrations of NH_3 of a sensor type D annealed at 480 °C.

When the test chamber where the sensors are kept was flushed with dry air, the sensors regained their baseline resistance, but this was a very slow process. The time needed for the sensors to reach the baseline was about one hour and half. This process could be speeded up by heating the sensors, at a

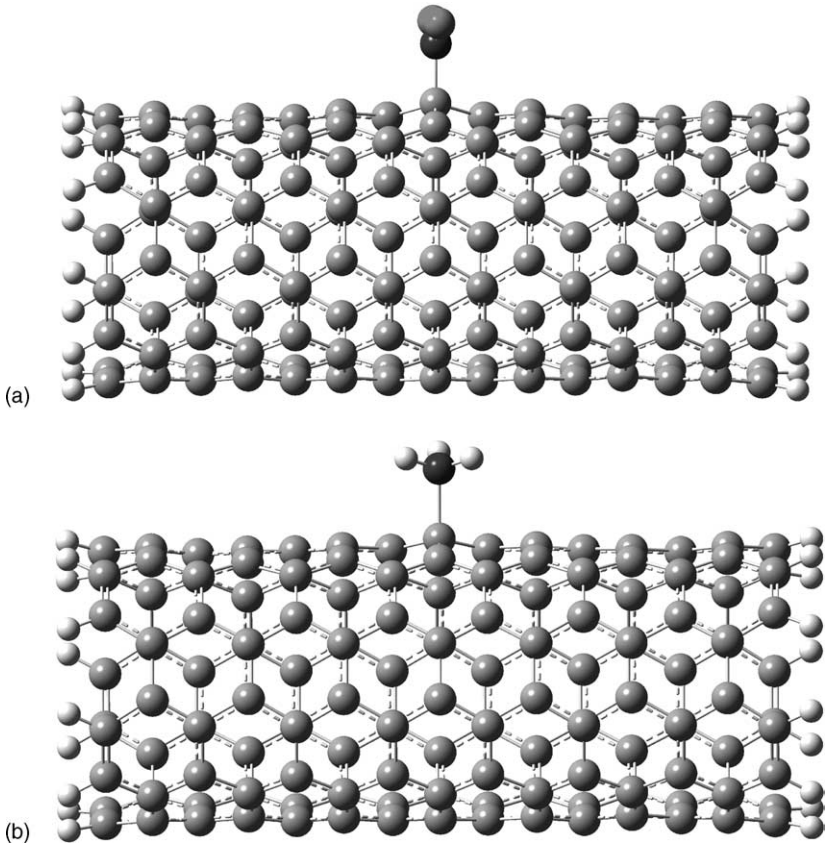

Fig. 8. Structures of the addition of NO_2 (a) and NH_3 (b) to the open single-walled (5,5) carbon nanotube with 150 carbon atoms and hydrogen terminated at the open ends used as a test system.

lower temperature than the one used for annealing the active film, during the cleaning phase.

4.3. Theoretical interpretation

In order to make a further interpretation of the results obtained, ab initio calculations were performed of the chemical addition for a number of functional groups to a (5,5) carbon nanotube, as mentioned above. First the interaction energy was calculated for the addition to the perfect side-wall for NO_2 and NH_3: being +21.4 and −26.0 kcal/mol, respectively (Fig. 8). For bonding to a perfect nanotube side-wall, an exothermic interaction is thus predicted for NO_2 as compared to an endothermic interaction for NH_3, although the interaction energy is relatively low for NO_2. Furthermore, as a clear interaction is seen between the nanotube material and NO_2 in relation to the amount of oxygen present in the sample (see above, sensors type B and C), the predicted interaction energy gives an indication that the NO_2 gas molecules will also interact with oxygen-containing functional groups present on the nanotube surface, or with defects present in the nanotube material, rather than with a perfect side-wall of the carbon nanotube material. In order to check these assumptions, a nanotube with a vacancy was considered. Functionalising this system at the vacancy with NO_2 or with NH_3 results in an interaction energy that is far more important, with values of +88.8 and +49.7 kcal/mol, respectively (see Fig. 9(a) and (b)). Even a stronger interaction energy (+177 kcal/mol) is found when the NO_2 group dissociates and one oxygen atom bonds to one carbon atom and the nitrogen is bound to the two other carbon atoms of the vacancy and to the second oxygen (see Fig. 9(c)). A so strong interaction energy is expected to be irreversible. This indicates that if vacancies were present in the body of the nanotubes, these would be functionalised by both NO_2 and NH_3 with a strong interaction as a result. However, as evidenced experimentally for NO_2, the gas sensor operation is reversible, while no clear interaction with the nanotubes is seen for NH_3 except when the nanotube material is partly destroyed (see above, sensor D), therefore a different type of interaction can be expected.

Treatment with oxygen plasma functionalises the carbon nanotubes with different types of oxygen-containing groups, as seen by XPS (see above and Ref. [31]). Upon longer plasma treatment, the relative occurrence of carbonyl groups rises while the quantity of hydroxyl groups lowers, although OH groups have higher interaction energy with a perfect nanotube wall as compared to other oxygen-containing functional groups [31]. However, when a vacancy is functionalised with a hydroxyl group, our calculations suggest a dissociation, with the oxygen atom bonding to two carbon atoms and the hydrogen to the third carbon atom of the vacancy. As oxygen plasma treatment is expected to create defects in the nanotube material such as vacancies, their functionalisation can indeed be expected to give rise to carbonyl groups rather than hydroxyl groups.

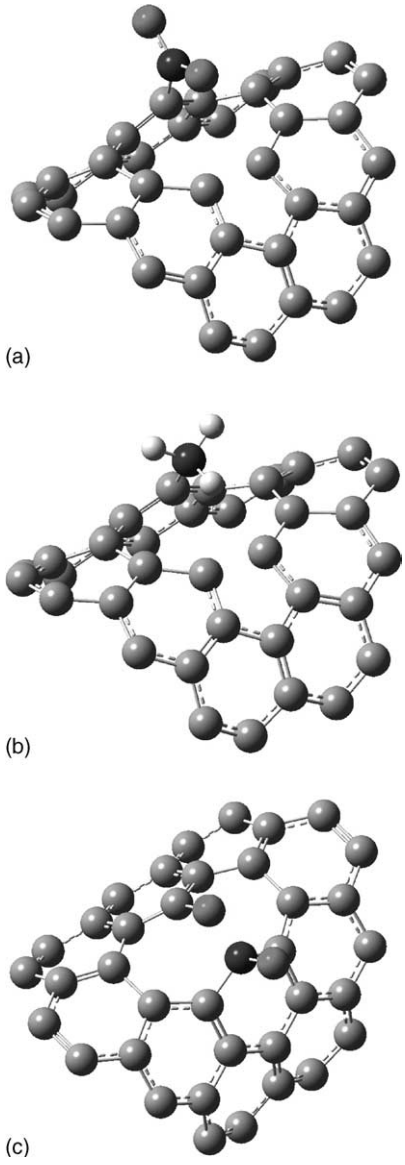

Fig. 9. Detailed view of the (5,5) carbon nanotube with a vacancy (one carbon atom removed), functionalised with (a) an NO_2 group, (b) an NH_3 group and (c) an NO_2 group dissociated on the vacancy, resulting in one oxygen atom bonded to one carbon atom and the nitrogen atom bounded to the two other carbon atoms of the vacancy and to the second oxygen.

In order to analyse this type of interaction, we estimated the interaction energy between this hydroxylated vacancy and NO_2 or NH_3 (see Fig. 10(a) and (b)). For the latter, an interaction energy of only 4.6 kcal/mol was found. This is in accordance with the experimental results showing no detection of NH_3 gas molecules by sensors type B and C. For NO_2, an interaction energy of 0 kcal/mol was found. As this is in clear contradiction with the experimental results, which showed a clear interaction with NO_2, this suggests that, additionally, another type of oxygen functionalisation has to be present at the surface of nanotubes.

If a vacancy is functionalised with O_2, dissociation is again observed, resulting in one C=O and one C–O–C func-

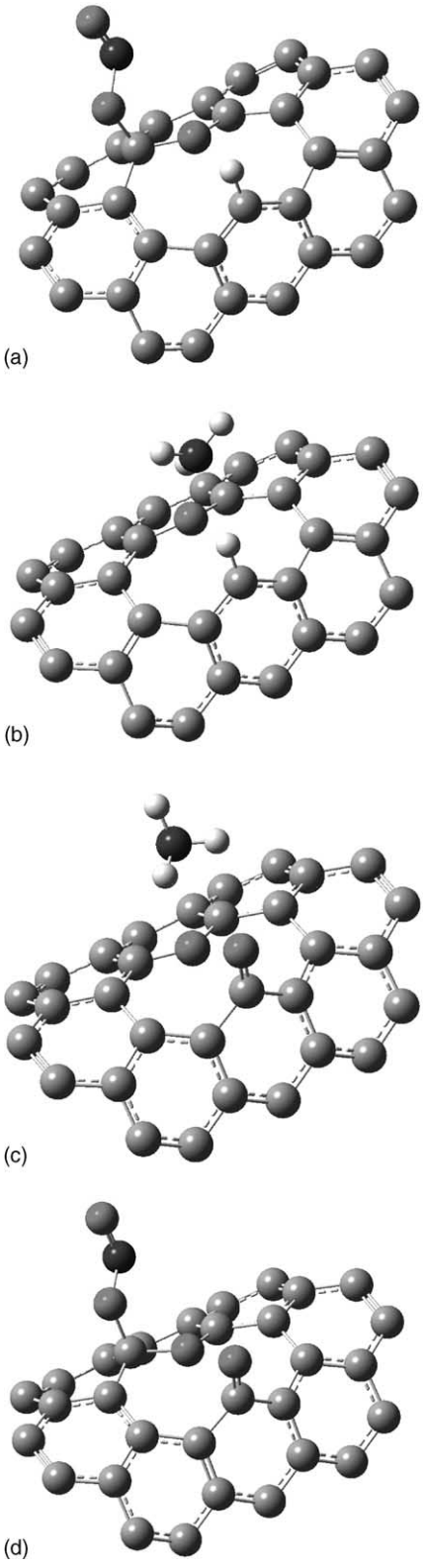

Fig. 10. Detailed view of the interaction between a (5,5) carbon nanotube with an OH functionalized vacancy with (a) an NO_2 group, or (b) an NH_3 group; and of an O_2 functionalised vacancy with (c) an NH_3 group, or (d) an NO_2 group.

tional group. Functionalisation of this oxygenated system results, once again, in an interaction energy of 4.6 for NH_3 (see Fig. 10(c)). However, for NO_2 an interaction energy of 48.3 kcal/mol is found (see Fig. 10(d)). This value is consistent with the clear but reversible interaction observed experimentally between the carbon nanotube material and NO_2 for sensors type B and C, for which no interaction was observed with NH_3. Interaction between gas molecules and carbon nanotube films is thus expected to occur in the proximity of oxygenated defects, such as vacancies, rather than at the carbon nanotubes themselves. This is consistent with the experimental result showing higher interaction of NO_2 upon oxygen increase. Besides defect site functionalisation, the oxygenation of carbon nanotubes end-sides can also be expected. However, due to the huge aspect ratio of the nanotube material, a larger interaction at the nanotube side walls can be expected as compared to the end-sides. As different structural defects or functional groups present in carbon nanotube films result in different interaction energies for NO_2 or NH_3, a better control over these features could further contribute to increase the performance of this type of carbon nanotube based gas sensors.

5. Conclusions

The detection of NO_2 and NH_3 at concentrations as low as 500 ppb and 200 ppm, respectively, was found to be possible at ambient temperature with MWNT-based gas sensors fabricated by the drop coating method. The films behaved similarly to p-type semiconductors in the presence of these gases.

Plasma treatment was found to improve the sensing potential of MWNT. Oxygen plasma functionalisation of MWNT proved to play an important role in their responsiveness to ammonia and nitrogen dioxide. The presence of oxygen at the surface of MWNT was found to increase their sensitivity to NO_2, and to lower the detection limit. On the other hand, the presence of metallic catalysts at the surface of nanotubes increased their sensitivity to NH_3.

Theoretical ab initio calculations predicted an exothermic interaction for functionalising a perfect nanotube side-wall with NO_2, as compared to an endothermic interaction for NH_3. Also, the interaction energy was calculated for a vacancy functionalised with an OH group and an O_2 molecule, both predicted to dissociate and form a carbonyl function on the nanotube. Functionalising this oxygenated vacancy with NO_2/NH_3 shows only a clear interaction for the O_2 functionalised vacancy with NO_2. The higher interaction energy predicted for functionalising an oxygenated vacancy, as compared to a perfect side-wall, is in accordance with the experimental results. These show a higher responsiveness when there is a higher presence of oxygen at the surface of nanotubes. The occurrence of oxygen-functionalised defects in nanotubes can be increased by increasing the duration of the oxygen plasma treatment.

Acknowledgements

We are grateful to Dr. C. Cané and Dr. I. Gràcia that are with the Centre Nacional de Microelectrònica (CNM-Barcelona) for providing us with the microhotplate transducers. This paper presents research results of the ENABLE project financed by the Région Wallone de Belgique and by the Spanish Commission for Science and Technology (CICYT) under grant no. TIC2003-06301. Parts of this work are also directly connected to the Belgian Program on Interuniversity Attraction Poles (PAI5/1/1) on Quantum Size Effects in Nanostructured Materials, to the 'Action de Recherche Concertée' entitled 'Interaction électron-phonon dans les nanostructures' sponsored by the Communauté Française de Belgique, and to the FAME European network of excellence. GVL and J-CC acknowledge the National Fund for Scientific Research [FNRS] of Belgium for financial support. EHE and ES acknowledge the University Rovira i Virgili for financial support.

References

[1] M. Terrones, A. Jorio, M. Endo, A.M. Rao, Y.A. Kim, T. Hayashi, H. Terrones, J.-C. Charlier, C. Dresselhaus, M.S. Dresselhaus, New direction in nanotube science, Mater. Today 7 (2004) 30–45.
[2] S. Iijima, Helical microtubules of graphitic carbon, Nature 354 (1991) 56–58.
[3] S.J. Tans, R.M. Verschueren, C. Dekker, Room temperature transistor based on a single carbon nanotube, Nature 393 (1998) 49–51.
[4] H. Dai, J.H. Hafner, A.G. Rinzler, D.T. Cobert, R.E. Smalley, Nanotubes as nanoprobes in scanning probe microscopy, Nature 384 (1996) 147–150.
[5] P. Poncharal, Z.L. Wang, D. Ugarte, W.A. de Heer, Electrostatic deflections and electrochemical resonances of carbon nanotubes, Science 283 (1999) 1513–1516.
[6] A.C. Dillon, K.M. Jones, T.A. Bekkedahl, C.H. Kiang, D.S. Bethune, M.J. Heben, Storage of hydrogen in single-walled carbon nanotubes, Nature 386 (1997) 377–379.
[7] L. Yukui, Z. Changchun, L. Xinghui, Field emission display with carbon nanotubes cathode: prepared by a screen-printing process, Diamond Relat. Mater. 11 (2002) 1845–1847.
[8] C.J. Lee, D.W. Kim, T.J. Lee, Y.C. Choi, Y.S. Park, W.S. Kim, Y.H. Lee, W.B. Choi, N.S. Lee, J.M. Kim, Y.G. Choi, S.C. Yu, Synthesis of uniformly distributed carbon nanotubes on a large area of Si substrates by thermal chemical vapor deposition, Appl. Phys. Lett. 75 (1999) 1721–1723.
[9] P. Kim, C.M. Lieber, Nanotube tweezers, Science 286 (1999) 2148–2150.
[10] P.G. Collins, K. Bradley, M. Ishigami, A. Zettl, Extreme oxygen sensitivity of electronic properties of carbon nanotubes, Science 287 (2000) 1801–1804.
[11] C. Journet, W.K. Maser, P. Bernier, A. Loiseau, M.L. de la Chapelle, S. Lefrant, P. Deniard, R. Lee, J.E. Fischer, Large scale production of single wall carbon nanotubes by the electric arc technique, Nature 388 (1997) 756–758.
[12] A. Thess, R. Lee, P. Nikolaev, H. Dai, P. Petit, J. Robert, C. Xu, Y.H. Lee, S.G. Kim, D.T. Colbert, G. Seuseria, D. Tomanek, J.E. Fischer, R.E. Smalley, Crystalline ropes of metallic carbon nanotubes, Science 273 (1996) 483–487.
[13] M. Terrones, N. Grobert, J. Olivares, J.P. Zhang, H. Terrones, K. Kordatos, W.K. Hsu, J.P. Hare, P.D. Townsend, K. Prassides, A.K. Cheetham, H.W. Kroto, D.R.M. Walton, Controlled production of aligned-nanotube bundles, Nature 388 (1997) 52–55.
[14] S. Fan, M.G. Chapline, N.R. Franklin, T.W. Tombler, A.M. Cassell, H. Dai, Self-oriented regular arrays of carbon nanotubes and their field emission properties, Science 283 (1999) 512–514.
[15] L. Valentini, C. Cantalini, L. Lozzi, I. Armentano, J.M. Kenny, S. Santucci, Reversible oxidation effects on carbon nanotubes thin films for gas sensing applications, Mater. Sci. Eng. C 23 (2003) 523–529.
[16] J. Li, Y. Lu, Q. Ye, M. Cinke, J. Han, M. Meyyappan, Carbon nanotube sensors for gas and organic vapor detection, Nano Lett. 3 (2003) 929–933.
[17] O.K. Varghese, P.D. Kichambre, D. Gong, K.G. Ong, E.C. Dickey, C.A. Grimes, Gas sensing characteristics of multi-wall carbon nanotubes, Sens. Actuators B 81 (2001) 32–41.
[18] S. Peng, J. O'Keeffe, C. Wei, K. Cho, J. Kong, R. Chen, N. Franklin, H. Dai, Carbon nanotube chemical and mechanical sensors, in: Proceedings of the Third International Workshop on Structural Health Monitoring, vol. 1, 2001, pp. 1–8.
[19] S.G. Wang, Q. Zhang, D.J. Yang, P.J. Sellin, G.F. Zhong, Multiwalled carbon nanotube-based gas sensors for NH_3 detection, Diamond Relat. Mater. 13 (2004) 1327–1332.
[20] C. Cantalini, L. Valentini, I. Armentano, L. Lozzi, J.M. Kenny, S. Santucci, Sensitivity to NO_2 and cross-sensitivity analysis to NH_3, ethanol and humidity of carbon nanotubes thin film prepared by PECVD, Sens. Actuators B 95 (2003) 195–202.
[21] H. Bubert, S. Haiber, W. Brandl, G. Marginean, M. Heintze, V. Brüser, Characterization of the uppermost layer of plasma-treated carbon nanotubes, Diamond Relat. Mater. 12 (2003) 811–815.
[22] N.O.V. Plank, R. Cheung, Functionalisation of carbon nanotubes for molecular electronics, Microelectron. Eng. 73/74 (2004) 578–582.
[23] T. Saito, K. Matsushige, K. Tanaka, Chemical treatment and modification of multi-walled carbon nanotubes, Phys. B: Condens. Matter 323 (2002) 280–283.
[24] A.T. Matveev, D. Golberg, V.P. Novikov, L.L. Klimkovich, Y. Bando, Synthesis of carbon nanotubes below room temperature, Carbon 39 (2001) 155–158.
[25] Z. Kónya, I. Vesselenyi, K. Niesz, A. Kukovecz, A. Demortier, A. Fonseca, J. Delhalle, Z. Mekhalif, J.B. Nagy, A.A. Koós, et al., Large scale production of short functionalized carbon nanotubes, Chem. Phys. Lett. 360 (2002) 429–435.
[26] K.S. Ahn, J.S. Kim, Ch. Ok Kim, J.P. Hong, Non-reactive rf treatment of multiwall carbon nanotube with inert argon plasma for enhanced field emission, Carbon 41 (2003) 2481–2485.
[27] Nanocyl S.A., http://www.nanocyl.com.
[28] G. Lefebvre, J. Verbist, Characterization of acrylonite plasma-polymerized on carbon fibres, Adv. Comp. Mater. Lett. 1 (1992) 34.
[29] E. Llobet, P. Ivanov, X. Vilanova, J. Brezmes, J. Hubalek, K. Malysz, I. Gràcia, C. Cané, X. Correig, Screen-printed nanoparticle tin oxide films for high-yield sensor microsystems, Sens. Actuators B 96 (2003) 94–104.
[30] M.J. Frisch, G.W. Trucks, H.B. Schlegel, G.E. Scuseria, M.A. Robb, J.R. Cheeseman, J.A. Montgomery, J.T. Vreven, K.N. Kudin, J.C. Burant, J.M. Millam, S.S. Iyengar, J. Tomasi, V. Barone, B. Mennucci, M. Cossi, G. Scalmani, N. Rega, G.A. Petersson, H. Nakatsuji, M. Hada, M. Ehara, K. Toyota, R. Fukuda, J. Hasegawa, M. Ishida, T. Nakajima, Y. Honda, O. Kitao, H. Nakai, M. Klene, X. Li, J. E. Knox, H.P. Hratchian, J.B. Cross, C. Adamo, J. Jaramillo, R. Gomperts, R.E. Stratmann, O. Yazyev, A. J. Austin, R. Cammi, C. Pomelli, J.W. Ochterski, P.Y. Ayala, K. Morokuma, G.A. Voth, P. Salvador, J.J. Dannenberg, V.G. Zakrzewski, S. Dapprich, A.D. Daniels, M.C. Strain, O. Farkas, D.K. Malick, A.D. Rabuck, K. Raghavachari, J.B. Foresman, J.V. Ortiz, Q. Cui, A.G. Baboul, S. Clifford, J. Cioslowski, B.B. Stefanov, G. Liu, A. Liashenko, P.

Piskorz, I. Komaromi, R.L. Martin, D.J. Fox, T. Keith, M.A. Al-Laham, C.Y. Peng, A. Nanayakkara, M. Challacombe, P.M.W. Gill, B. Johnson, W. Chen, M.W. Wong, C. Gonzalez, Pople, J.A., Gaussian, Inc., Pittsburgh, PA, 2003.

[31] A. Felten, C. Bittencourt, G. Van Lier, J.C. Charlier, J.J. Pireaux, RF-plasma functionalisation of carbon nanotubes surface: O_2, NH_3, CF_4 treatment, J. Appl. Phys., submitted for publication.